HOSTED BY

ELSEVIER

Available online at www.sciencedirect.com

ScienceDirect

Journal of Magnesium and Alloys ■■ (2017) ■■–■■
www.elsevier.com/journals/journal-of-magnesium-and-alloys/2213-9567

Full Length Article

Microstructure evolution and mechanical properties of hot deformed Mg9Al1Zn samples containing a friction stir processed zone

E. Cerri [a,*], D. Knez [b], T. Rimoldi [a], M.T. Di Giovanni [a]

[a] D.I.A. Università di Parma, via G. Usberti 181/A, 43124, Parma, Italy
[b] FELMI-ZFE, Steyrergasse 17, 8010, Graz, Austria

Received 22 September 2017; revised 13 November 2017; accepted 17 November 2017

Available online

Abstract

During the last decade, FSP of magnesium alloys has become more popular due to the potential microstructure refinement of their eutectic phases, and interest has increased around the AZ1 that is one of the most commercially used magnesium alloys. In this work, high pressure die cast AZ91 plates were tensile tested at high temperatures after friction stir processing (FSP), with the stirred region in the middle of the gauge length. Samples deformed at 350 °C revealed an increment of ductility that was doubled as compared to those deformed at 300 °C and a strengthening of the nugget was measured by Vickers microhardness (HV). The correlation of HV average values to local grain size confirmed the validity of the Hall–Petch type equation where stress is replaced by hardness. X-rays diffraction and electrical conductivity highlighted the potential increment of solute atoms in solid solution during FSP. Scanning Electron Microscopy (SEM) and Transmission Electron Microscopy (TEM) investigations performed on as-FSPed and hot deformed samples determined MgAlZn and AlMn particles type evolution through statistical analysis that supported mechanical properties and the strengthening mechanisms.

Keywords: AZ91; Friction stir processing; Mechanical properties; Microstructure; SEM; TEM

1. Introduction

The need of metallic materials with high specific mechanical properties for the transportation industry has brought Mg alloys to be one of the candidates for their low density and elevated specific strength. Several efforts have been made to improve the ductility of Mg and its alloys: because of the hexagonal close packed crystalline structure, their ductility is lower compared to other alloy systems, i.e. aluminium alloys. Physical metallurgy principles state that fine grain size improves strength, ductility and the formability at high temperatures. Most of the Mg alloy components are produced by die casting, but to achieve a fine microstructure, a severe plastic deformation (SPD) process is required. Among several SPD techniques, friction stir processing (FSP) is becoming increasingly successful [1–3]. The microstructure is refined and, in case of cast or powder metallurgy materials, densification is achieved. Moreover, the tuning of FSP parameters controlling the amplitude and the depth of the processed region and the mechanical properties, resulting from the refined microstructure, are finalized.

During the last decade several papers have been published about the effect of FSP on mechanical properties and microstructure of Mg–Al alloys. It has been shown that FSP can refine the grain dimension to submicron size, break up and partially dissolve the intermetallic and secondary phases [4]. The mechanical behaviour is improved at room temperature by FSP due to elongation increases caused by texture modification [5–7] and grain size strengthening [8]. Anyway, room temperature ductility usually remains lower than 10%, while significant increase in elongation (>>10%) or superplastic behaviour is achieved in Mg alloys with refined grain size tested at high temperatures, as shown in a number of published papers [9–11]. In those manuscripts and others [12–14], usually the tensile samples are directly machined from the stirred region and present a homogeneous microstructure along the gage length; the grain size results strictly related to the FSP parameters (rotational rate and advancing speed). In another paper [15], a superplastic behaviour is achieved just through a solution

* Corresponding author. Università di Parma, G. Usberti 181/A, 43124 Parma, Italy.
E-mail address: emanuela.cerri@unipr.it (E. Cerri).

https://doi.org/10.1016/j.jma.2017.11.003

Table 1
Sample designation and surface nugget temperature.

FSP condition	2500 rpm, 30 mm/min	2500 rpm, 50 mm/min	3000 rpm, 30 mm/min	3000 rpm, 50 mm/min
Sample designation	2500-30	2500-50	3000-30	3000-50
Surface nugget temperature [°C]–[°K]	228–501	198–471	265–538	248–521

treatment of the die cast alloy, reducing the dimension and the amount of the intermetallic phases before applying FSP.

One of the most popular Mg–Al alloys is the AZ91 (Mg–9Al–1Zn). Its success among other Mg alloys comes from the optimal balance of several technological properties such as: castability, mechanical strength, corrosion resistance, crack resistance and ductility. AZ91 components are usually produced by die casting but, enhanced mechanical properties are achieved by high pressure die casting (HPDC) due to higher solidification rate as compared to more traditional die casting technologies. For these reasons, the AZ91 is the perfect candidate to exploit for the comprehension of fundamental relationships between microstructure and technological properties. In this light, FSP was applied to AZ91 HPDC plates as microstructure refining technology to gather results on mechanical properties resulting at room and high temperatures [16–19]. The aim of this paper was to find the relationships between mechanical properties and the microstructure of the most characteristic FSPed regions by using electron microscopy investigation techniques, image analysis, microanalysis and electro conductivity measurements.

2. Materials and methods

A high-pressure die casting AZ91 magnesium alloy plate with a thickness of 3 mm was used in the as cast condition. The chemical composition (in weight %) is Mg-8,9%Al-0,79%Zn-0,24%Mn.

The plates were friction stir processed by an AISI 521 (or H13) tool steel pin with a truncated cone geometry, having a shoulder diameter of 15 mm and a height of 2.3 mm. Two pin rotation rates, ω (2500 and 3000 rpm) and two advancing speeds, v (30 and 50 mm/min) were applied as processing conditions. The FSP was carried out for one pass on a steel backing plate. A K-type thermocouple was held in contact with the stirred region behind the pin to measure the temperature during the process. Sample designation and temperatures are illustrated in Table 1.

Specimens for tensile tests were machined from FSPed plates in order to have the loading axis normal to the stirring direction. Each FSPed sample was deformed at 300 °C and 10^{-3} s^{-1}. Furthermore, the 2500-30 samples were tensile tested also at 300 °C, 10^{-4} s^{-1} and 350 °C.

Vickers microhardness measurements (HV) were performed by a load of 300 g for 15 s in the plane perpendicular to the stirring direction and at different depths from the upper surface: at 0.5 mm (top), at 1.5 mm (centre) and at 2 mm (bottom).

Electrical conductivity measurements were carried out on the clean surface of samples by a SIGMATEST device based on Eddy current principle.

The microstructure on cross-sectional planes of friction stir processed samples was examined by optical microscopy (OM), SEM and TEM. For OM and SEM observations, samples were mechanically polished to 1 μm with alcohol based diamond polishing paste and etched in a solution of 10 ml acetic acid, 4 g

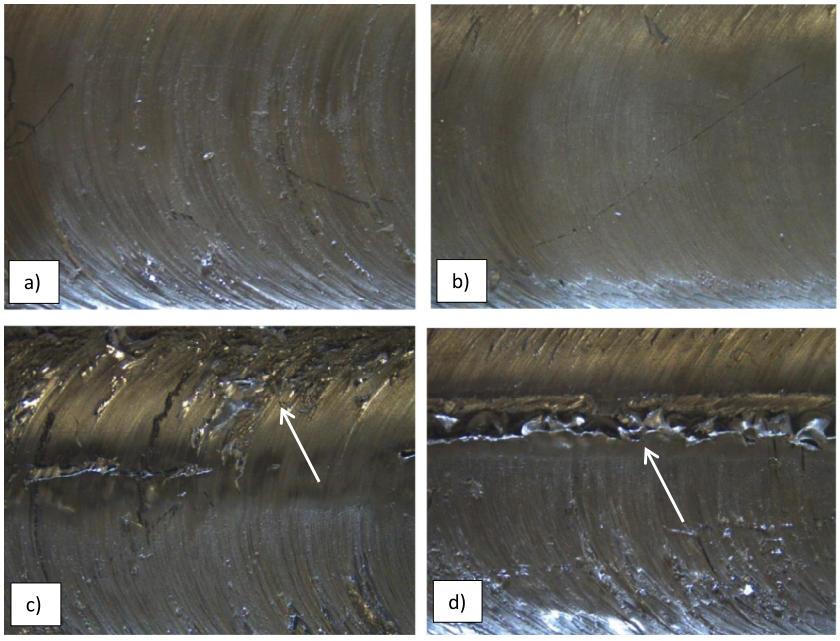

Fig. 1. Optical microscopy (OM) images showing features of the upper stirred zone: surface roughness or onion rings in (a) 2500-30 and (b) 2500-50 samples; lack of fill defects in (c) 3000-30 and (d) 3000-50 as shown by white arrows.

Please cite this article in press as: E. Cerri, D. Knez, T. Rimoldi, M.T. Di Giovanni, Microstructure evolution and mechanical properties of hot deformed Mg9Al1Zn samples containing a friction stir processed zone, Journal of Magnesium and Alloys (2017), doi: 10.1016/j.jma.2017.11.003

picric acid, 50 ml ethanol and 25 ml distilled water. Grain size statistics were measured by OM on a population of at least 100 grains in the nugget, in the heat affected zone (HAZ) and base material (BM) regions.

Thin foils for TEM observations were cut and mechanically thinned in a Gatan dimple grinder until a thickness of approximately 3 μm was reached. The final thinning of the samples was performed in a Gatan Precision Ion Polishing System (PIPS™). This system houses two Ar-ion guns which were set to an angle of 6° from below and 4° from above the sample plane with an acceleration voltage set to 4 kV. The sample was kept rotating during milling at a speed of 1 rpm. TEM characterisation of the samples started immediately after the final thinning step. During transfer from the PIPS to the microscope vacuum, the samples had to be shortly (<5 min) exposed to ambient conditions to avoid oxidation.

TEM observations were carried out by a FEI TF20 and a FEI TITAN^3 G2 operating at 200 kV and 300 kV, respectively, to study the morphology and distribution of precipitates and examine the microstructure at a fine level.

Phase identification was also carried out by X-rays diffractometer using a Cu_α radiation tube working at 30 mA and 40 kV with a measure step of 0.05° for 20 s.

3. Results

3.1. Friction stir processed samples

The surface quality of the FSP samples is illustrated in Fig. 1. The 2500-30 and 2500-50 specimens have smooth surfaces with no macroscopic defects (Fig. 1a,b). At a higher rotation rate, surface galling defects appear in the FSPed region (Fig. 1c) probably generated by metal sticking to the pin tool because of excessive temperature. Moreover a macroscopic "surface lack of fill" defect is detectable all along the stir direction (Fig. 1d) due to an insufficient flow arm formation across top surface. The temperatures measured on the stirred surfaces 10 mm beyond the pin (Table 1) are 40–50 °C higher for 3000-samples compared to 2500-samples, confirming the type of defects. It is expected that these macroscopic defects induce a reduction in mechanical properties; because of that a greater emphasis has been placed on 2500-rpm samples rather than 3000-rpm ones.

Samples with smooth surface were sectioned in the plane perpendicular to the stirring direction to check the underlying material; Fig. 2a shows a low magnification picture highlighting the material flow in the nugget cross-section of 2500-30 sample. In thermo-mechanically affected zone (TMAZ) of advancing side (red rectangle in Fig. 2a), dark regions are observed that could foresee defects, but at higher magnification (Fig. 2b) just one tunnel of 50–60 μm width is observed.

In order to have an exhaustive microstructure characterisation, grain sizes were measured in the nugget region at three depths from the upper surface, i.e. at 0.5 mm (top), at 1.5 mm (centre) and at 2 mm (bottom) of 2500-30 and 2500-50 samples. The statistical distributions of equivalent grain diameters (EGD) were reported in Fig. 3. For both samples, at the centre and bottom regions, EGD distributions are shifted

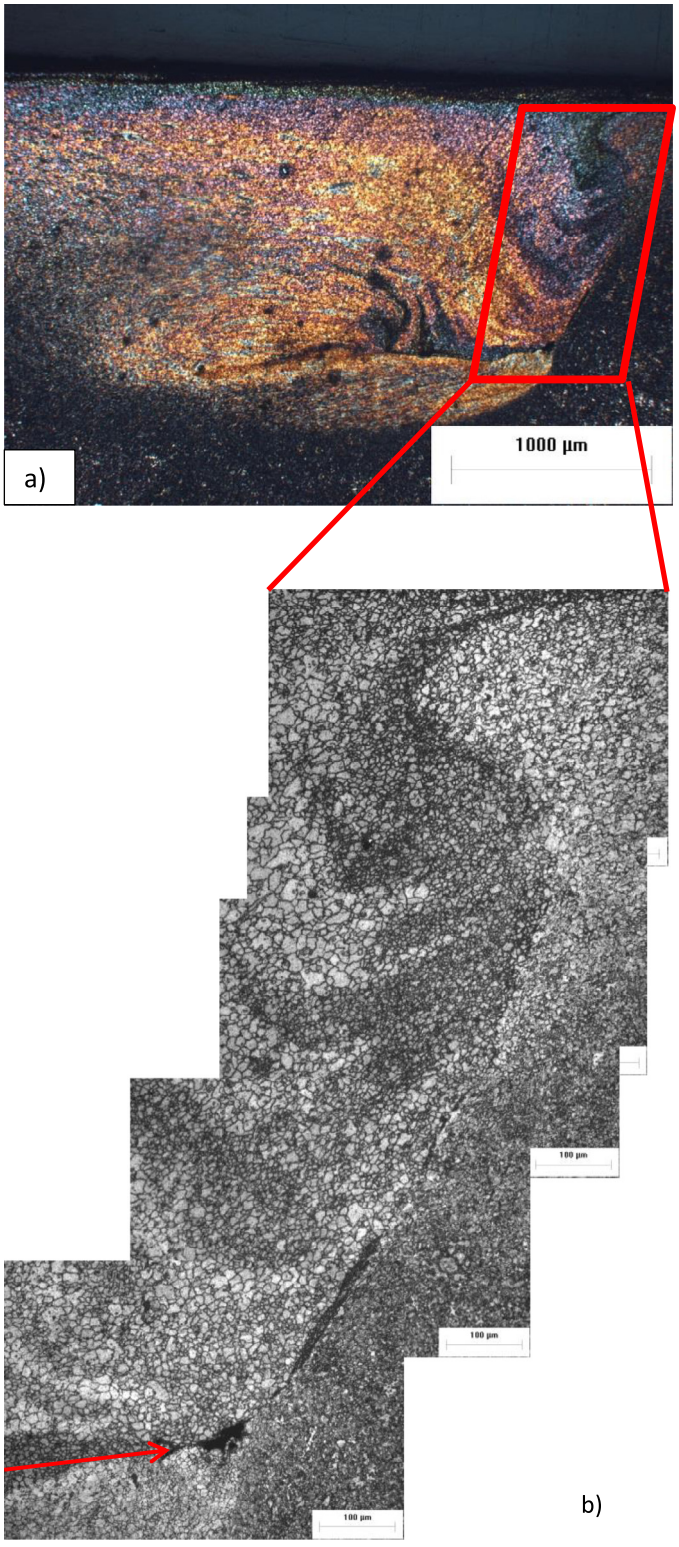

Fig. 2. OM images of the transverse section in 2500-30 sample showing: a) whole FSPed area and b) Thermo Mechanically Affected Zone (TMAZ) with a tunnel defect (red arrow).

2–3 μm to lower values compared to the top. In detail in 2500-30 sample, the most likely EGD is 12–13 μm at the top and decreases to 9–10 μm at the centre and bottom with a frequency of 60%–70% in each distribution. In the 2500-50

Please cite this article in press as: E. Cerri, D. Knez, T. Rimoldi, M.T. Di Giovanni, Microstructure evolution and mechanical properties of hot deformed Mg9Al1Zn samples containing a friction stir processed zone, Journal of Magnesium and Alloys (2017), doi: 10.1016/j.jma.2017.11.003

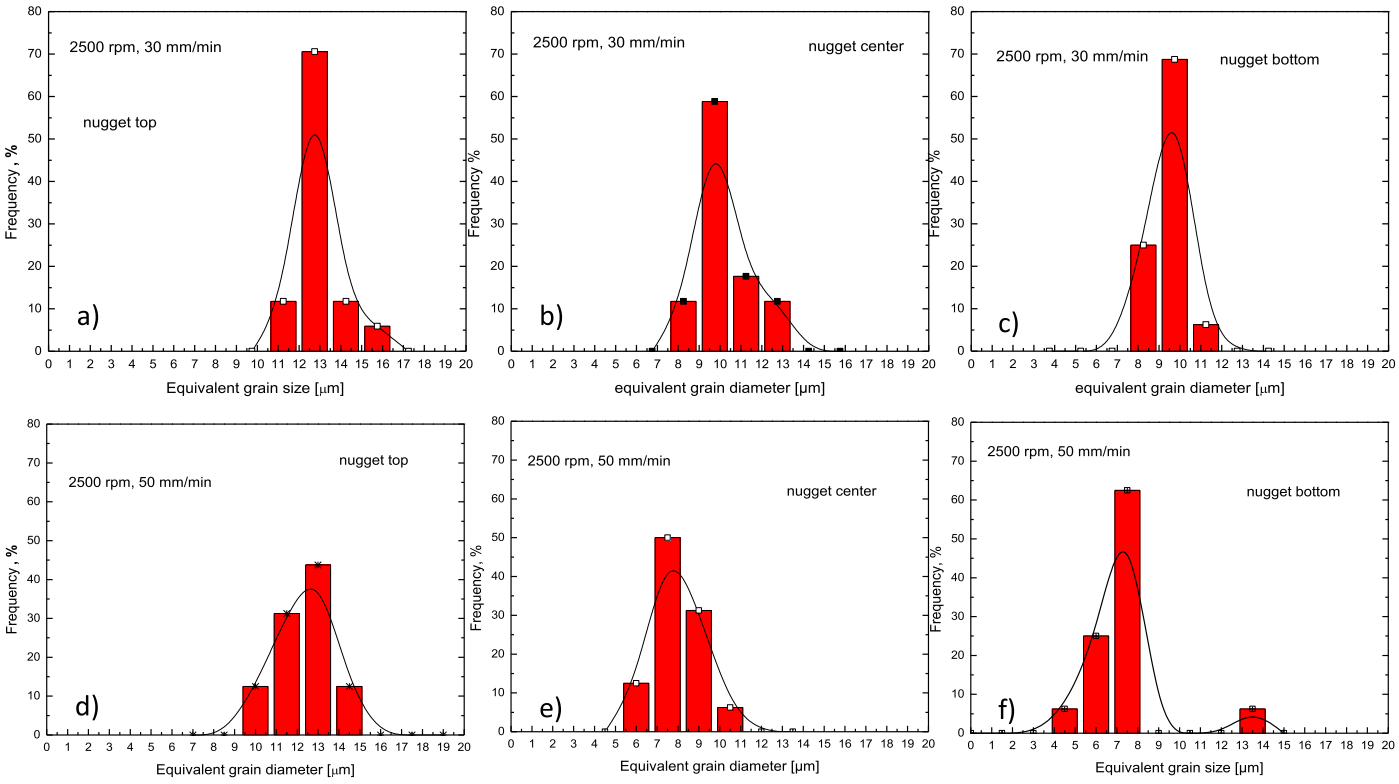

Fig. 3. Comparison of equivalent grain diameter (EGD) distributions as measured at the top (a, d), centre (b, e) and bottom (c, f) in the nugget zone of 2500-30 (upper row) and 2500-50 (lower row) samples.

sample, the EGD distribution at the top is smoother around 12–13 μm (frequency of 40%) and the most likely EGD values decrease to 7–8 μm at centre and bottom regions.

With the increase of advancing speed from 30 to 50 mm/min, the growth kinetics of recrystallized grains (i.e. EGD) slows down due to the lower heat input and the local temperature decrease, being temperature proportional to ω^2/v [20]. As result, the EGD distributions for 2500-50 sample are shifted by 2 μm towards lower values compared to 2500-30 samples.

XRD was performed on FSPed samples to investigate, at a first stage, the microstructure modifications induced by the stirring process. Fig. 4a illustrates XRD peaks for 2500-30 and for the BM as reference sample. In the 2500-30 sample (Fig. 4a, red line), the intensity of β peaks decreases and α-Mg peaks are shifted to lower theta with respect to reference positions of BM (Fig. 4a, black line), i.e. the d_{hkl} spacings have increased. A rough estimation of strain ε accumulated during the FSP was performed according to the following equation [21]:

$$\varepsilon = \frac{\Delta d}{d} = -ctg(\theta)\cdot\Delta\theta$$

where d and θ are the interplanar distance and the diffracted angle, respectively, of the main α-Mg peak (i.e. (1,0,−1,1) or (101) plane) in BM while Δd and Δθ are the interplanar distance and peak-angle shifts of 2500-30 compared to BM (Fig. 4b).

In this case:

$$\Delta\theta = \|36,78° - 36,65°\| = 0,13°,\ \theta = \theta_{BM} = \frac{36,78°}{2} = 18,39°$$

and $ctg\theta = 3,008$

and the result of "residual strain" is $\varepsilon_{2500\text{-}30} = \frac{\Delta d}{d} = \|-cotg\theta\cdot 0,13°\| = 0,391$.

The estimated value of "residual strain" $\varepsilon_{2500\text{-}30}$ (i.e. increase in the interplanar distance in (1,0,−1,1) α-Mg peak) is correlated to the severe plastic deformation induced by the stirring process in the magnesium matrix that promotes the build-up of defects such as dislocations and increment of atoms in solid solution. The intensity of β-peaks decreases in the 2500-30 sample as compared to BM (taking into account also the background), that means dissolution of the β eutectic phase in the matrix occurred. In this context, the shift of α-Mg peaks can be ascribed to the increased solute concentration in the magnesium matrix compared to BM, as confirmed by EDS analysis reported in [17].

The HV_{FSP}/HV_{BM} microhardness ratios of measures, performed at the top and centre of the section perpendicular to the stirring direction, are shown in Fig. 5 (solid lines) for 2500-30 sample as function of the distance from the nugget centre by assuming $HV_{BM} = 70HV$. The HV profiles decline 10% in the nugget region (from −5 mm to +5 mm) compared to areas out of stirred region. This is justified by volume reduction of the hard intermetallic network after FSP i.e. the partial dissolution

Please cite this article in press as: E. Cerri, D. Knez, T. Rimoldi, M.T. Di Giovanni, Microstructure evolution and mechanical properties of hot deformed Mg9Al1Zn samples containing a friction stir processed zone, Journal of Magnesium and Alloys (2017), doi: 10.1016/j.jma.2017.11.003

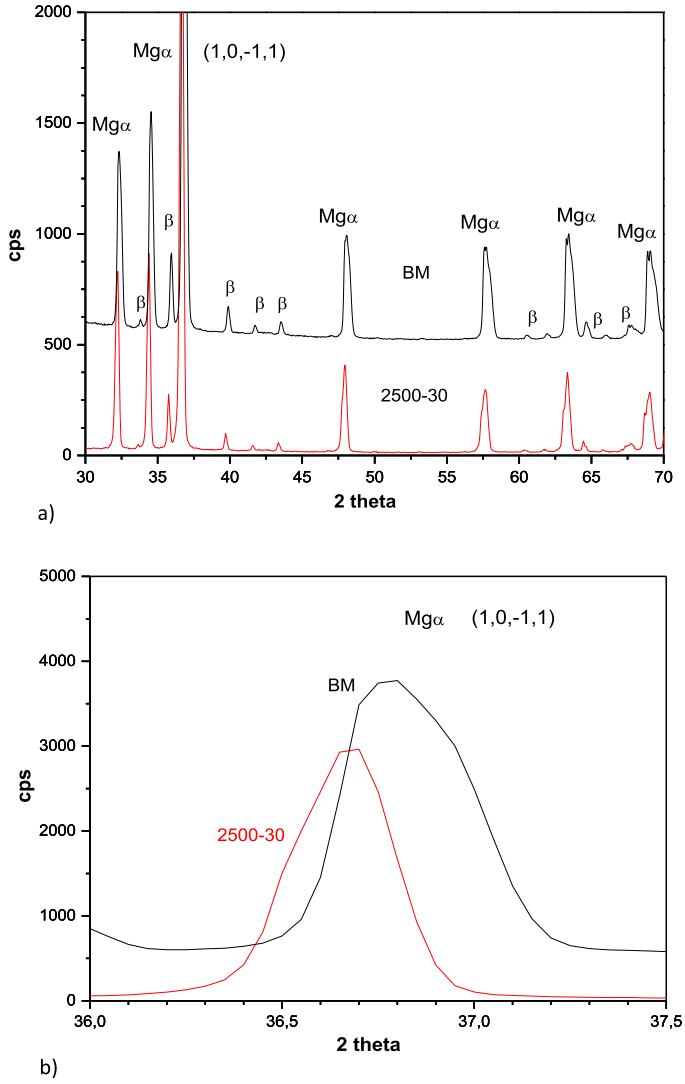

Fig. 4. X-ray diffractometry of nugget regions showing a) β − phase and α-Mg peaks evolution in 2500-30 sample with respect to the base material (BM) and b) the shift of the main α-Mg peak in 2500-30 with respect to the base material (BM).

of β-phase and the α-Mg peak shift, as indicated by XRD analysis (Fig. 4a) and by SEM microanalysis in [18]. A further proof of the increase of solute atoms concentration in the nugget is the related decrease of electrical conductivity values considering the same area (dotted lines in Fig. 5); at 8 mm far from the centre of the nugget the electrical conductivity attains BM values.

In the attempt to correlate Vickers microhardness to grain size, evaluations of average grain dimensions were carried out on small areas ($100 \times 100\ \mu m^2$) below HV marks. By using Hall–Petch type relations, i.e. $HV \cong HV_0 + kd^{-1/2}$, where HV_0 and k are constant for the material, the graph in Fig. 6 shows a good linear fit for all the FSP conditions used in this work with values of $HV_0 = (41 \pm 5)$ MPa and $k = (76 \pm 10)$ MPa/μm½; these results are in good agreement with Chang et al. [8] for the AZ31. Differences in grain size were ruled by friction stir process parameters (rotational rate and advancing speed) especially inside the nugget zones (top, centre and bottom).

Tensile properties of the 2500-30 sample were evaluated at room and at high temperatures to investigate the deformation behaviour after FSP, as discussed in [18]. For completeness, graphs showing sigma peak (maximum tensile strength) and epsilon values ($\ln(1+e)$ where e is the % engineering elongation) as function of temperature and strain rate are given in Fig. 7. At room temperature, a peak stress of 180 MPa is shown (Fig. 7a) but a poor ductility of $\varepsilon = 0.015$ is measured. At high temperatures (300 °C and 350 °C), tensile peak stress decreases with temperature from 60 to 35 MPa at $10^{-3}\ s^{-1}$ and, from 20 to 12 MPa at $10^{-4}\ s^{-1}$. The elongation to fracture, that increases with temperature and decreases with strain rate, shows an important enhancement up to $\varepsilon \cong 0.16$ during deformation at 350 °C and $10^{-4}\ s^{-1}$; this value is an excellent result considering that tensile samples, used in these experiments, have the FSPed region in the middle of their gauge length (they are not mini specimen extracted from the nugget). The ductility declines to $\varepsilon \cong 0.07$ when the specimen is deformed at lower temperature (300 °C).

After deformation at 350 °C and $10^{-4}\ s^{-1}$, microhardness profiles were measured along the tensile axis, in the plane perpendicular to the stirring direction (same plane as in Fig. 5). The results (Fig. 8) show that profiles overlap along the tensile axis regardless the distance from the surface (top, centre or bottom). Moreover, there is a hardness increase in the nugget area (from 70 to 80 HV), except in correspondence of the TMAZ-HAZs, where relative minima appear. The direct comparison to HV profile before hot deformation (as FSPed) illustrates, actually, the drop in the TMAZ-HAZ regions and the rise of HV in the stirred area. Furthermore, the contribution to final elongation is more evident from the BM beyond the advancing side, while the retreating side area remains almost unstrained as shown in the picture of Fig. 8.

To investigate the mechanism of fracture, optical microscopy was performed on longitudinal sections of higher ductile samples (300 °C and 350 °C at $10^{-4}\ s^{-1}$) whose pictures are shown in Fig. 9 and 10. In the sample deformed at 300 °C and $10^{-4}\ s^{-1}$ three main regions are detectable close to fracture surface: i) an upper region (illustrated in Fig. 9a and labelled "a" region in Fig. 9d) that appears very dense of precipitates homogeneously distributed in the Mg-α matrix, ii) a middle region (Fig. 9b and "b" in Fig. 9d) 2 mm far away from fracture showing precipitates and magnesium matrix with apparently no precipitation and, iii) a region representing the transition from region "a" towards the bottom of the nugget (Fig. 9c and "c" in Fig. 9d) that illustrates the change from homogeneous precipitation to rough phases. The transition area is characterised by particles aligned along the material flow and also by voids whose diameters range from 30 to few μm. Voids were not observed in other zones at these magnifications.

The sample deformed at 350 °C (Fig. 10) has the highest ductility but the deformation is not homogenous along the gauge length, as previously shown in Fig. 8. The contribution to deformation is greater in the region adjacent to the advancing side, as illustrated in Fig. 10d. Optical microscopy shows i) an upper zone close to fracture (Fig. 10a and "a" region in Fig. 10d) with homogeneous precipitation – at least at this

Please cite this article in press as: E. Cerri, D. Knez, T. Rimoldi, M.T. Di Giovanni, Microstructure evolution and mechanical properties of hot deformed Mg9Al1Zn samples containing a friction stir processed zone, Journal of Magnesium and Alloys (2017), doi: 10.1016/j.jma.2017.11.003

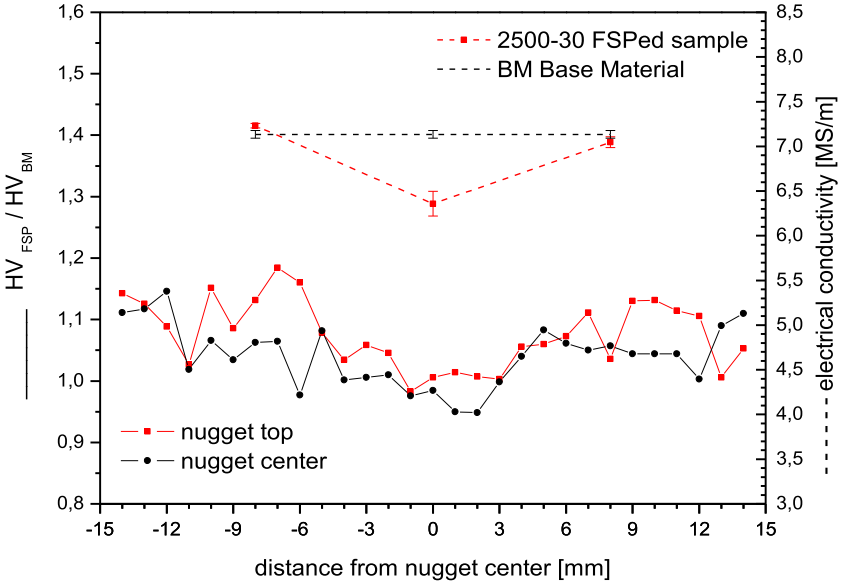

Fig. 5. Vickers microhardness and electrical conductivity measures of 2500-30 and base material (BM) samples. Vickers microhardness is displayed as HV_{fsp}/HV_{BM} ratio (BM = 70 HV).

magnification – ii) a central region, 500 μm far away from fracture (Fig. 10b and "b" region in Fig. 10d) with high precipitation density alternated to α-Mg matrix and, iii) a fracture zone (Fig. 10c and indicated as "c" in Fig. 10d) showing irregular cracks and porosities in the precipitate thick zone.

Fracture surfaces observed by SEM are illustrated in Fig. 11. The sample "2500-30" tensile tested at room temperature ($\varepsilon < 0.02$) shows a ductile fracture (Fig. 11a and b) with dimples and voids; fracture occurred out of the nugget and mostly at the border of HAZ and BM.

The hot deformation at 300 °C induces a fracture surface with voids and oxides (Fig. 11c) in the upper region of the fractured nugget; a similar microstructure is found at the bottom of the fracture surface but with a different material flow trend (Fig. 11d). By increasing the deformation temperature to 350 °C (strain rate = 10^{-4} s^{-1}), the ductility doubled to $\varepsilon \cong 0.14$ and dimples become clearly visible with particles inside (Fig. 11e). High magnification dimples and fractured filaments typical of superplastic behaviour are shown in Fig. 11f. The filaments are usually formed by a liquid phase originated from incipient melting but, in these experiments the temperature of 350 °C is below the melting temperature of AZ91 that is 420 °C [22]. It can be argued that the filaments originated from deformation around particles and tearing, due to stress concentration. Moreover, large areas with cleavage planes were detected in the fracture surfaces.

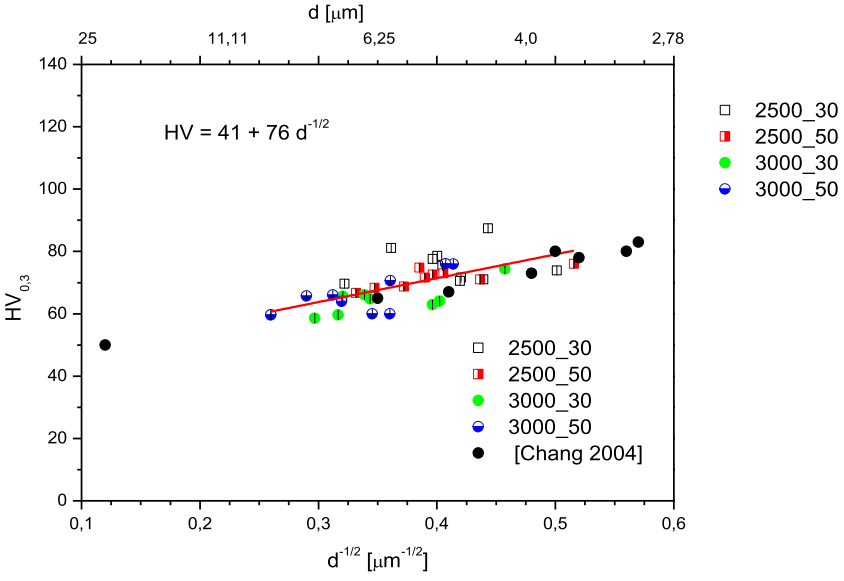

Fig. 6. Relationship among Vickers Hardness (HV) and grain diameter (d) as measured in different areas of the FSPed samples.

Please cite this article in press as: E. Cerri, D. Knez, T. Rimoldi, M.T. Di Giovanni, Microstructure evolution and mechanical properties of hot deformed Mg9Al1Zn samples containing a friction stir processed zone, Journal of Magnesium and Alloys (2017), doi: 10.1016/j.jma.2017.11.003

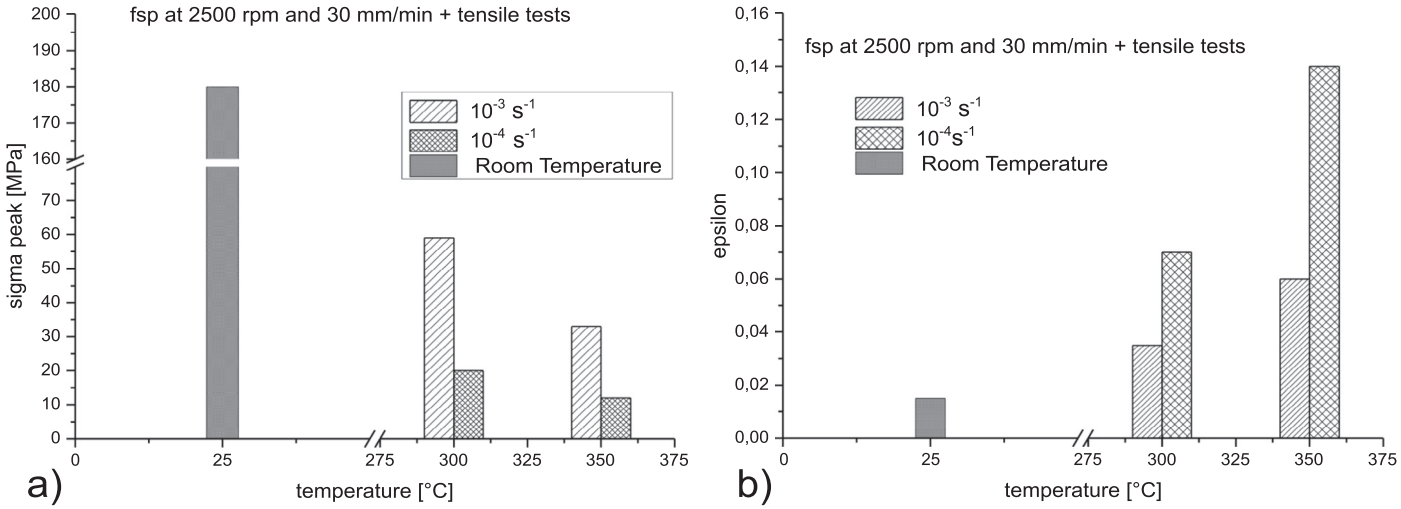

Fig. 7. Variation of tensile properties of 2500-30 samples as a function of temperature at constant strain rate. a) Sigma peak and b) epsilon (strain to failure).

3.2. Transmission electron microscopy

Samples obtained from FSPed cross sections were observed by TEM and STEM to study particle kinetics during exposure at the high temperatures of deformation tests. Fig. 12 illustrates the results of 2500-30 sample while Fig. 13 and 14 of 2500-30 samples tensile tested at 300 °C and 350 °C respectively at a strain rate of $10^{-4}\,s^{-1}$. Fig. 12a shows discontinuous (DP) and continuous precipitation (CP) of MgAlZn type particles while Fig. 12b shows a higher magnification of the CP zone. The grain boundary separating DP and CP regions is distinguishable by the presence of particles along the corrugated border. The DP particles may have a rounded shape after FSP. Smaller precipitates (Fig. 12c) also contain Mg, Al and Zn as shown by EELS spectrum. EELS elemental map sharpens Zn element evidence. A statistical evaluation of equivalent particle diameter (EPD) of particles found in Fig. 12a–d has been carried out with the purpose of studying their subsequent evolution during hot deformation. Statistical distributions are shown in Fig. 12 e–g and the average dimensions and inter-particle distances are listed in Table 2.

TEM observations of particles in FSPed AZ91 lead to distinguish three main populations: i) the discontinuous precipitated particles, such as the big phases in Fig. 12a, ii) elongated particles such as in Fig. 12b and c and, iii) very fine AlMn particles in Fig. 12d.

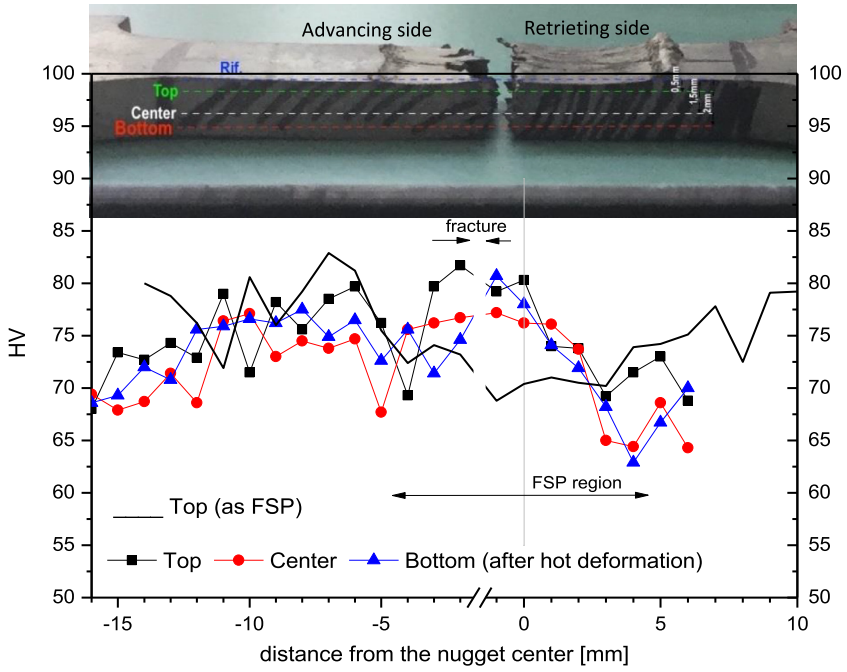

Fig. 8. Vickers microhardness of the 2500-30 sample measured at top, centre and bottom, as shown in the upper micrograph, after deformation at 350 °C and 10^{-4} s^{-1}. The advancing and retreating sides are indicated in the picture.

Please cite this article in press as: E. Cerri, D. Knez, T. Rimoldi, M.T. Di Giovanni, Microstructure evolution and mechanical properties of hot deformed Mg9Al1Zn samples containing a friction stir processed zone, Journal of Magnesium and Alloys (2017), doi: 10.1016/j.jma.2017.11.003

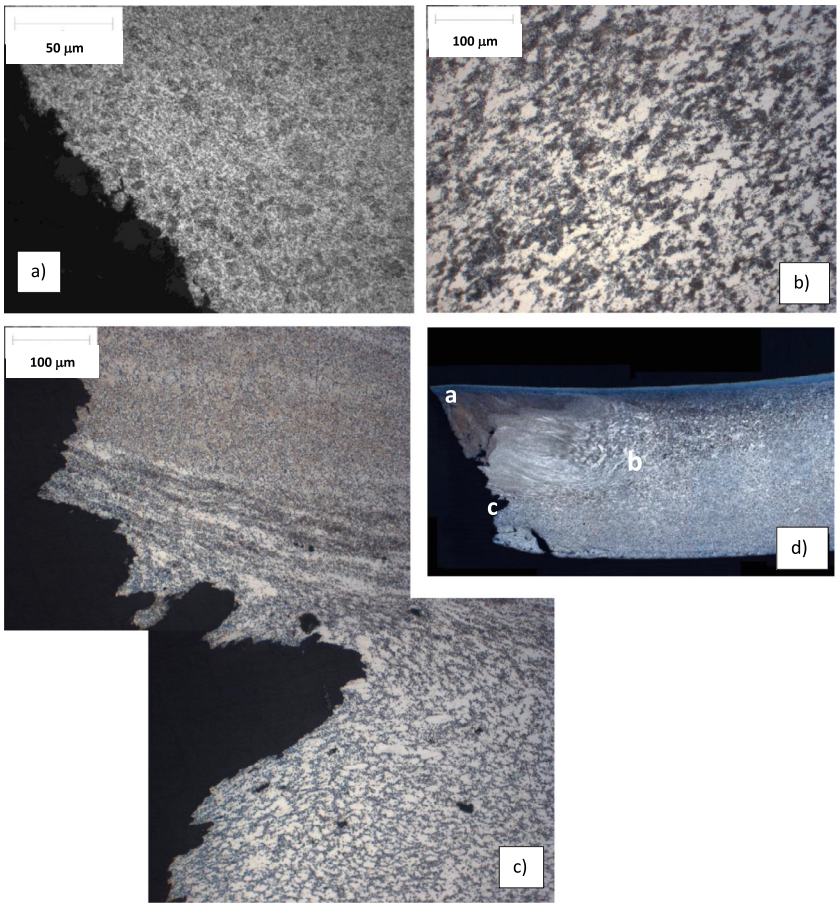

Fig. 9. Optical micrographs showing fracture region in 2500-30 sample after tensile deformation at 300 °C and $10^{-4}\,s^{-1}$. a) Micrograph of the "a" region in picture d); b) lower bound of the nugget, representative of "b" area in d); c) right side of the nugget, as shown in "c" zone of picture d).

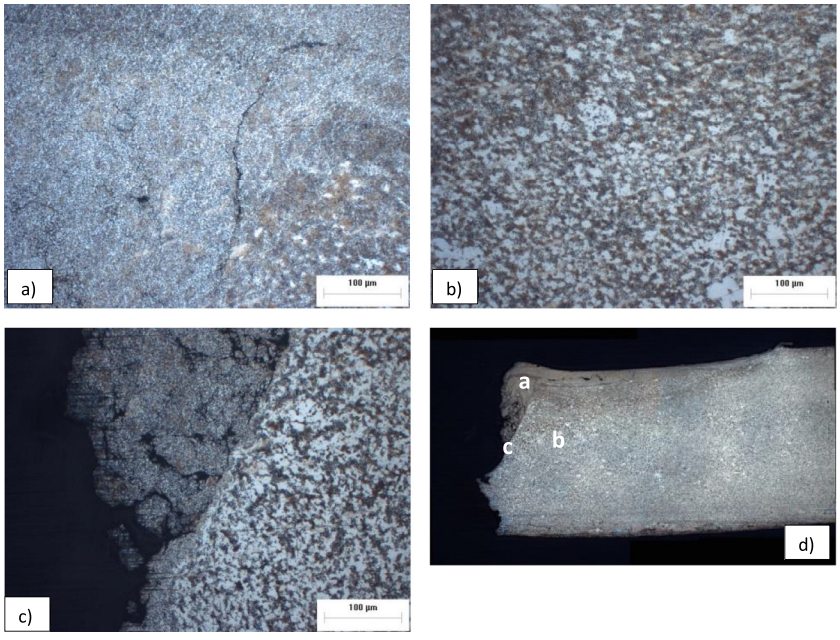

Fig. 10. Optical micrographs showing the fracture region in 2500-30 sample after tensile deformation at 350 °C and $10^{-4}\,s^{-1}$. a) Micrograph representative of the "a" region in picture d); b) right side of the nugget, as shown in "b" zone of picture d); c) lower bound of the nugget representative of "c" area in d).

Please cite this article in press as: E. Cerri, D. Knez, T. Rimoldi, M.T. Di Giovanni, Microstructure evolution and mechanical properties of hot deformed Mg9Al1Zn samples containing a friction stir processed zone, Journal of Magnesium and Alloys (2017), doi: 10.1016/j.jma.2017.11.003

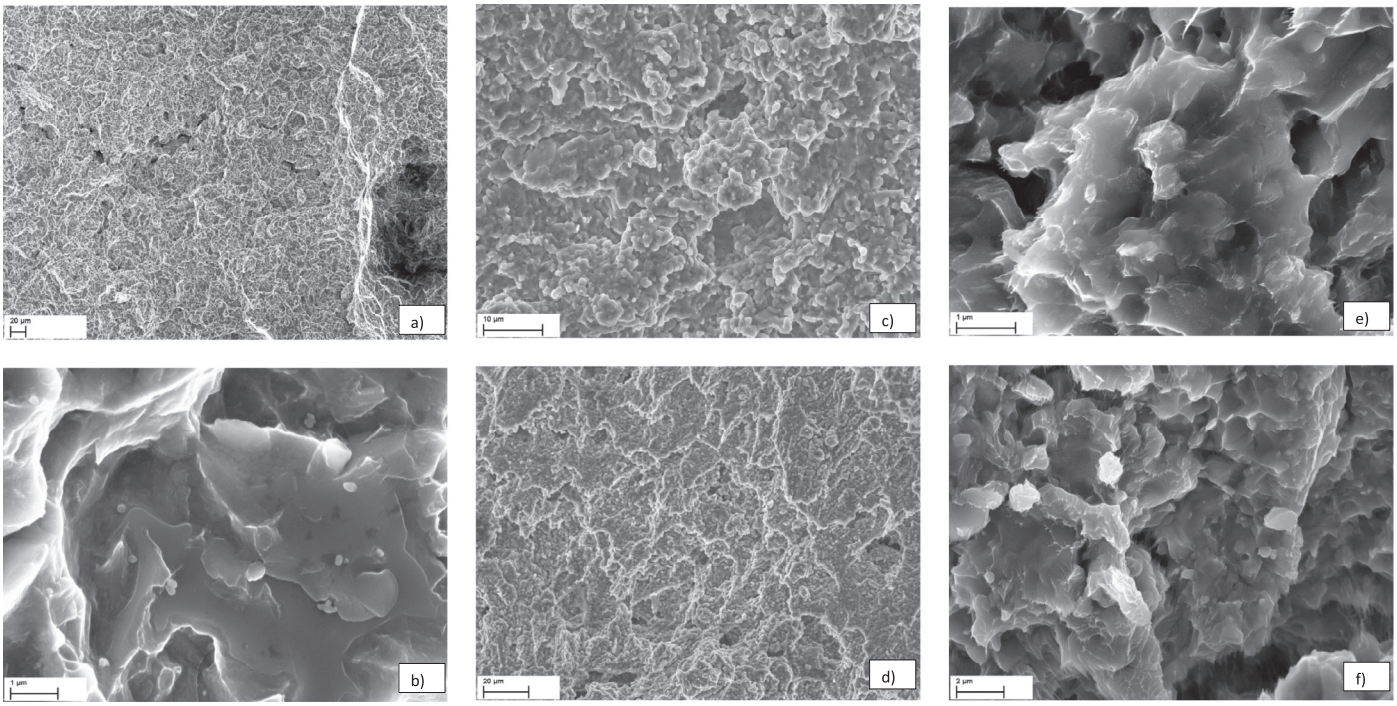

Fig. 11. Fracture surfaces of 2500-30 sample after different conditions of deformation. a) Dimples and voids and b) particles inside dimples after room temperature tensile test. After hot deformation at 300 °C and 10^{-4} s^{-1} showing voids and oxides c) at the top and d) at the bottom of the fracture surface. After hot deformation at 350 °C, 10^{-4} s^{-1} showing e) dimples and f) filaments.

DP particles in Fig. 12a present a wide EPD distribution with average size of 280 ± 150 nm (Fig. 12e). The EPDs of CP particles measured at different magnifications are comparable (Fig. 12f and g) but their inter-particle distances change from 120 ± 10 nm to 175 ± 50 nm. According to [23,24], the projected dimensions (length and width) onto the habit planes could determine differences in dimensions of up to 20% while variations in inter-particle spacing has to be related to different times of precipitation.

After hot deformation at 300 °C and 10^{-4} s^{-1}, DP particles (Fig. 13a) have spheroidized as demonstrated by their statistical distribution (Fig. 13e) that sharpens around the average size of 230 ± 80 nm. The increased EPD of CP particles (Fig. 13b and c) from 80–90 nm to 110–120 nm (Fig. 13f) and their related inter-particle distance of 260–280 nm testify the coarsening of elongated particles (Fig. 13b and c). In Fig. 13c, the EDS microanalysis confirms the presence of Zn in rounded MgAlZn type particles (spectrum 1 and 2) and Mg in the matrix (spectrum 3). Fig. 13d shows very fine AlMn type particles, whose statistical EPD distribution is illustrated in Fig. 13g; their size has decreased to 10 nm compared to 20 nm measured in the FSPed sample (Table 2).

By increasing temperature of deformation to 350 °C, average EPD of DP particles (Fig. 14a) decreases to 170 nm as attested by Fig. 14e. The CP particles (Fig. 14b) slightly reduced their size to 100 nm (Fig. 14f) and AlMn type (Fig. 14c) to 7 nm (Fig. 14g).

The graph in Fig. 15 illustrates the EPD averages with their associated errors as function of experimental conditions. For DP particles and AlMn type phases, the decrease with rising temperature of deformation is relevant while in CP particles, the variation of EPD with temperature is below the error bars and remains almost constant. On the contrary, the inter-particle spacing increases with temperature compared to the as FSP sample, testifying independent precipitation process occurring during hot deformation. The reduction in EPD size for DP and

Table 2
Average particle size and inter-particle distance.

2500-30 samples	DP particles average EPD [nm]	CP particles		AlMn particles average EPD [nm]
		Average EPD [nm]	Inter-particle distance [nm]	
as FSP	*280 ± 100	†90 ± 40	120 ± 10	≅ 20
		‡80 ± 30	175 ± 50	
+300 °C, 10^{-4} s^{-1}	230 ± 80	120 ± 40	260 ± 70	¶10 ± 2
		§110 ± 50	280 ± 50	
+350 °C, 10^{-4} s^{-1}	170 ± 60	100 ± 30	330 ± 90	7.0 ± 1.5

* From micrograph a), †from b), ‡from Fig. c) of Fig. 12.
§ From micrograph c) and ¶d) of Fig. 13.

Please cite this article in press as: E. Cerri, D. Knez, T. Rimoldi, M.T. Di Giovanni, Microstructure evolution and mechanical properties of hot deformed Mg9Al1Zn samples containing a friction stir processed zone, Journal of Magnesium and Alloys (2017), doi: 10.1016/j.jma.2017.11.003

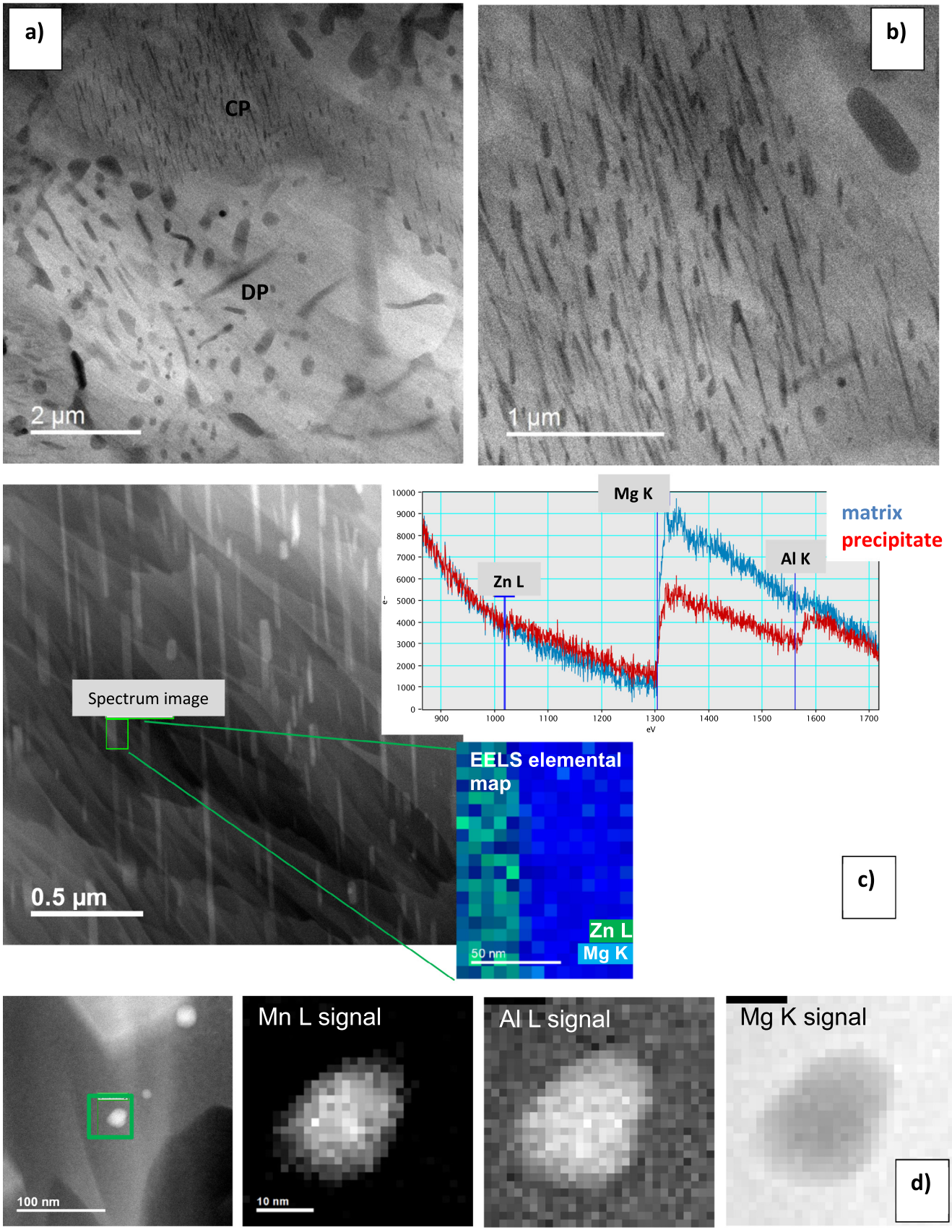

Fig. 12. TEM pictures (a-d) and statistical distributions of equivalent particle diameter (EPD) (e-g) of 2500-30 sample (as-FSPed). a) Discontinuous and Continuous precipitation (DP and CP) regions separated by a grain boundary. b) High magnification micrograph of a CP region. c) EELS spectrum and elemental map of a continuous precipitated particle (MgAlZn type). d) AlMn particles with elemental maps. e) EPD distribution of DP in a). f) EPD distribution of CP in b). g) EPD distribution of CP in c).

Please cite this article in press as: E. Cerri, D. Knez, T. Rimoldi, M.T. Di Giovanni, Microstructure evolution and mechanical properties of hot deformed Mg9Al1Zn samples containing a friction stir processed zone, Journal of Magnesium and Alloys (2017), doi: 10.1016/j.jma.2017.11.003

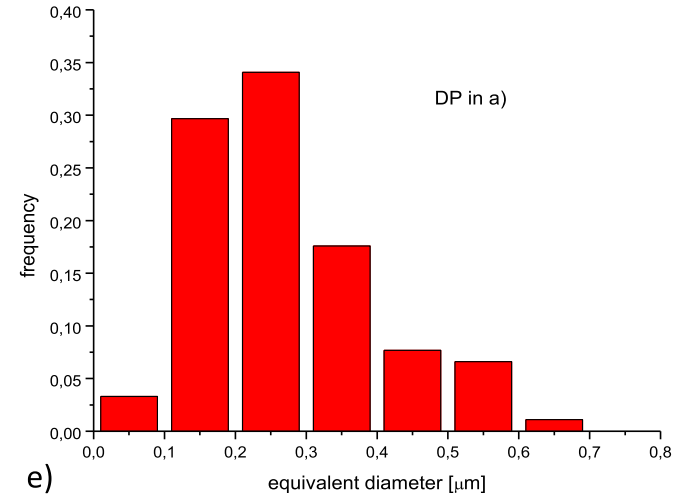

e)

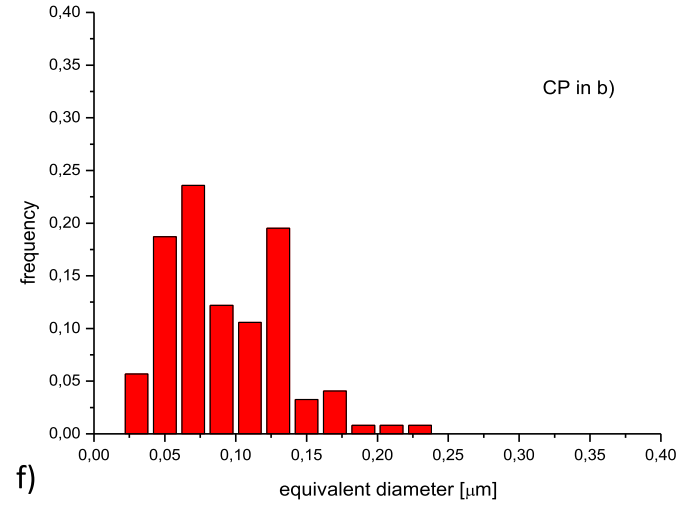

f)

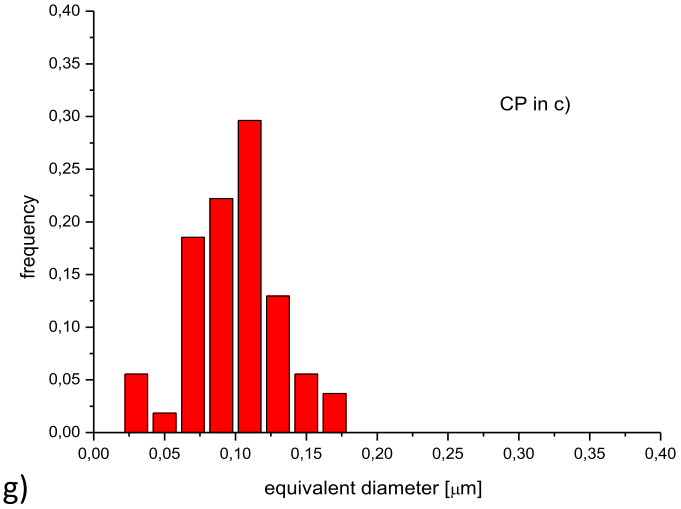

g)

Fig. 12. (*continued*)

AlMn type particles measured after hot deformation at 350 °C (as shown in Fig. 15) certainly contributes to the increase of HV in the nugget with respect to the as FSPed sample, as shown in Fig. 8. The contribution to the strengthening of AlMn particles at both room and elevated temperatures has been argued also by Zeng et al. [25].

Anyway, as CP particles were distributed more homogenously in the matrix than other types and no evidence of

Please cite this article in press as: E. Cerri, D. Knez, T. Rimoldi, M.T. Di Giovanni, Microstructure evolution and mechanical properties of hot deformed Mg9Al1Zn samples containing a friction stir processed zone, Journal of Magnesium and Alloys (2017), doi: 10.1016/j.jma.2017.11.003

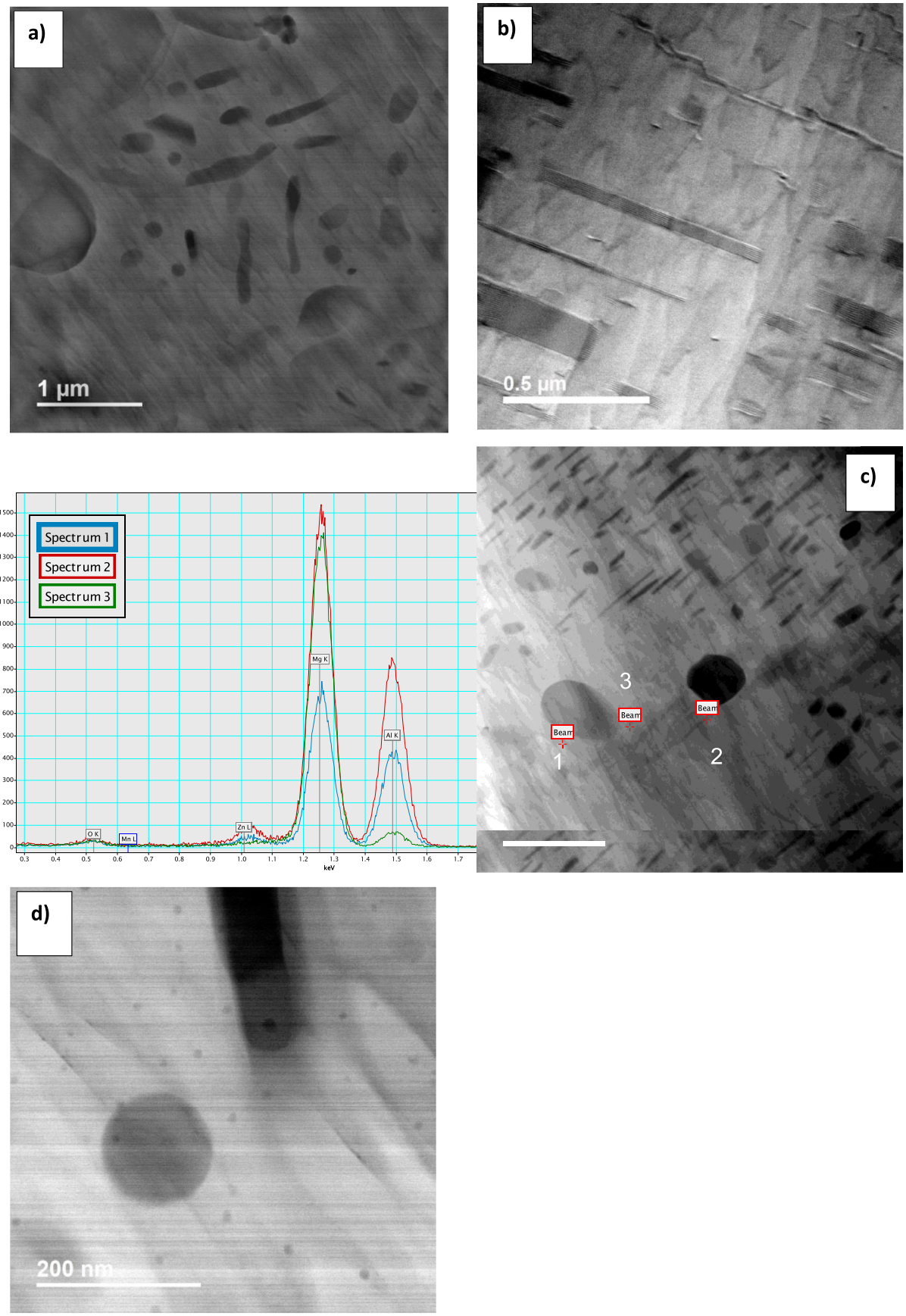

Fig. 13. TEM pictures (a-d) and statistical distributions of equivalent particle diameter (EPD) (e–g) of the sample hot deformed at 300 °C and 10^{-4} s^{-1} . a) Discontinuous precipitated particles. b) Continuous precipitated particles. c) Rounded particles with EDS spectrum showing MgAlZn type. d) High magnification TEM picture with fine AlMn particles. e) EPD distribution of DP in a). f) EPD distribution of CP in c). g) EPD distribution AlMn in d).

Please cite this article in press as: E. Cerri, D. Knez, T. Rimoldi, M.T. Di Giovanni, Microstructure evolution and mechanical properties of hot deformed Mg9Al1Zn samples containing a friction stir processed zone, Journal of Magnesium and Alloys (2017), doi: 10.1016/j.jma.2017.11.003

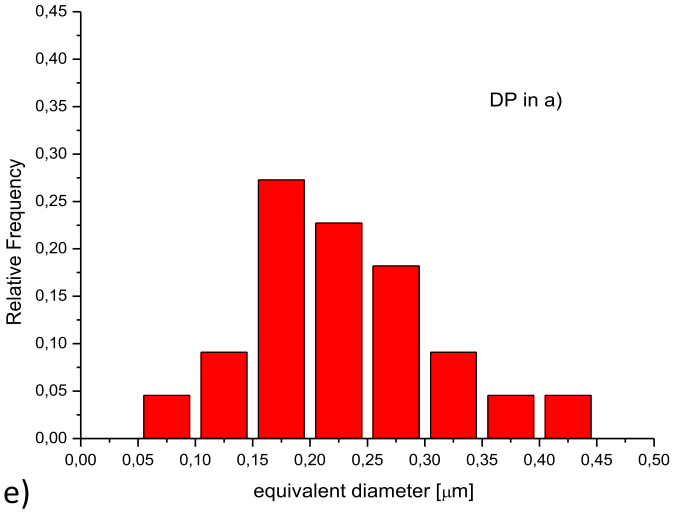

e)

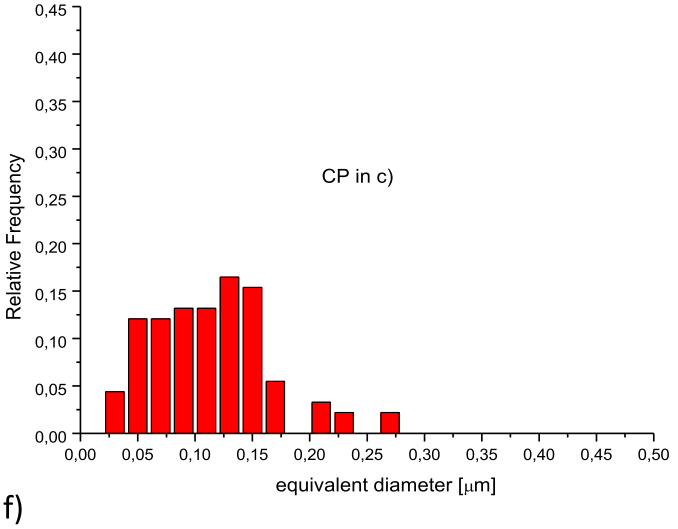

f)

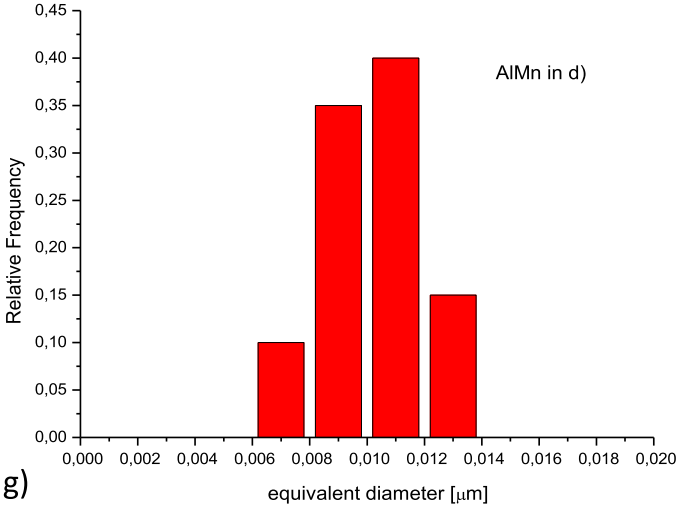

g)

Fig. 13. (*continued*)

Please cite this article in press as: E. Cerri, D. Knez, T. Rimoldi, M.T. Di Giovanni, Microstructure evolution and mechanical properties of hot deformed Mg9Al1Zn samples containing a friction stir processed zone, Journal of Magnesium and Alloys (2017), doi: 10.1016/j.jma.2017.11.003

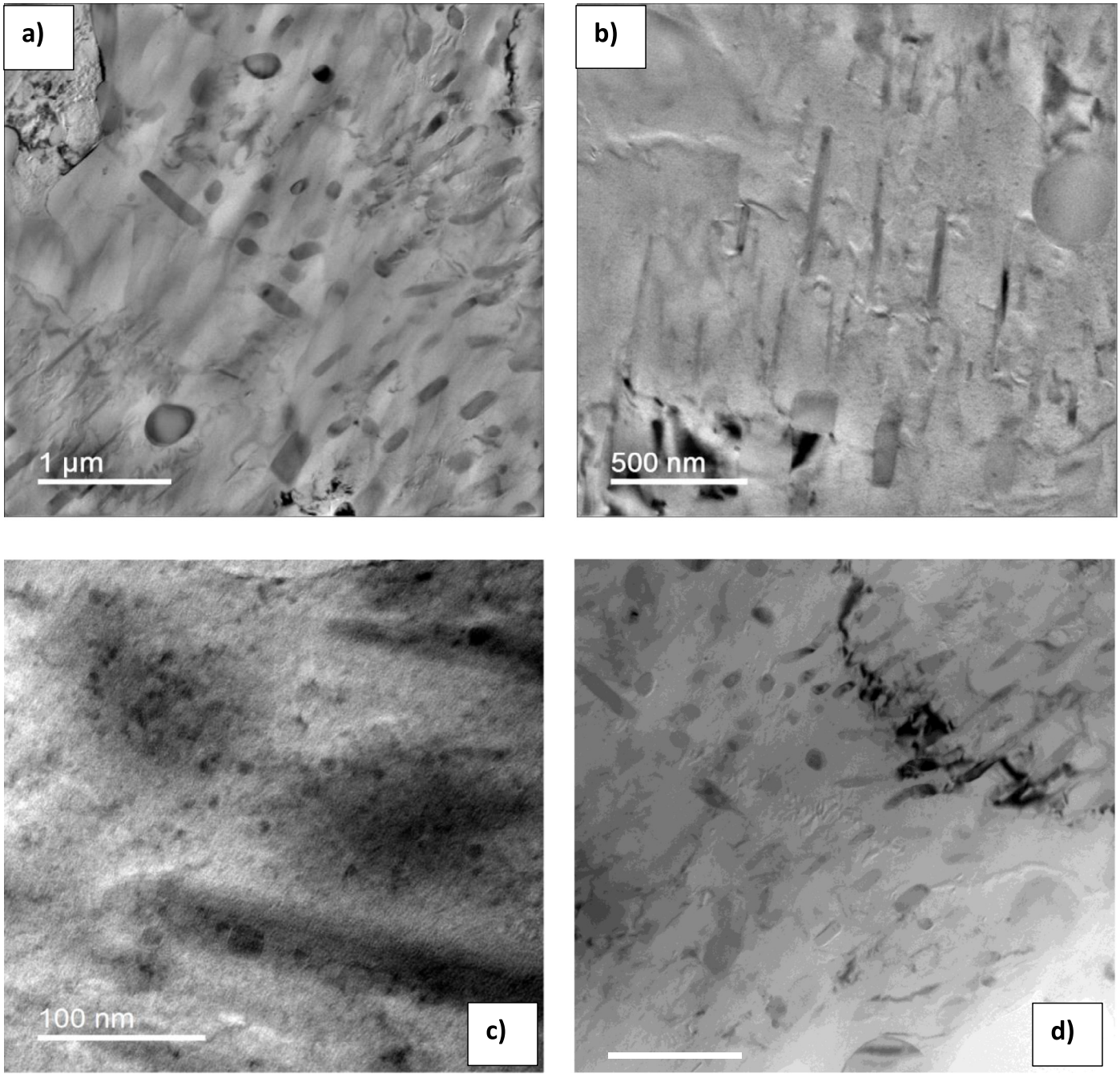

Fig. 14. TEM pictures (a–d) and statistical distributions of equivalent particle diameter (EPD) (e-g) of the sample tensile tested at 350 °C and 10^{-4} s^{-1} . a) Discontinuous precipitated particles. b) Continuous precipitated particles. c) High magnification TEM picture of very fine AlMn particles. d) Same region as a) showing the grain boundary. e) EPD distribution of DP in a). f) EPD distribution of CP in b). g) EPD distribution of AlMn of picture c).

particle cutting by dislocations was observed, they were considered in the calculation – based on Orowan mechanism – for strengthening contribution. According to precipitate-dislocation interaction theory and by considering the interaction of particles with dislocations in the basal plane of the hexagonal magnesium cell, the stress contribution can be approximated by the following formula [26–28]:

$$\sigma_{Or} = \frac{MGb}{2\pi\sqrt{1-\nu}} \frac{1}{l} \ln\left(d_p/b\right)$$

where M is the Taylor factor, G is the shear modulus of the matrix (17 GPa for magnesium), b is the Burgers vector of the dislocation (3.2 10^{-10} m), ν is the Poisson's ratio (0.35), d_p is the equivalent particle diameter and l is the mean inter-particle spacing.

The calculation of the ratio between σ_{Or} for 350 °C tensile tested sample and σ_{Or} for the 2500-30 one (by using the interplanar spacing for CP particles) gives ≅ 0.37. On the other hand, the ratio between the measured strengths of these samples (Fig. 7) is ≅ 0.09 thus it is very different from the prediction that

Please cite this article in press as: E. Cerri, D. Knez, T. Rimoldi, M.T. Di Giovanni, Microstructure evolution and mechanical properties of hot deformed Mg9Al1Zn samples containing a friction stir processed zone, Journal of Magnesium and Alloys (2017), doi: 10.1016/j.jma.2017.11.003

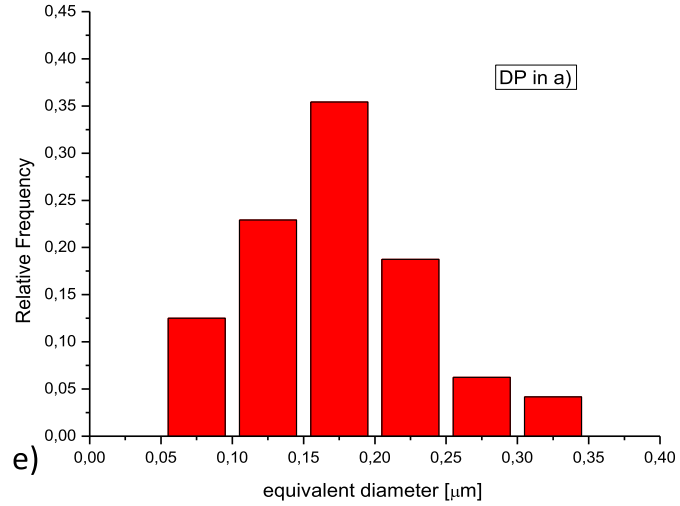

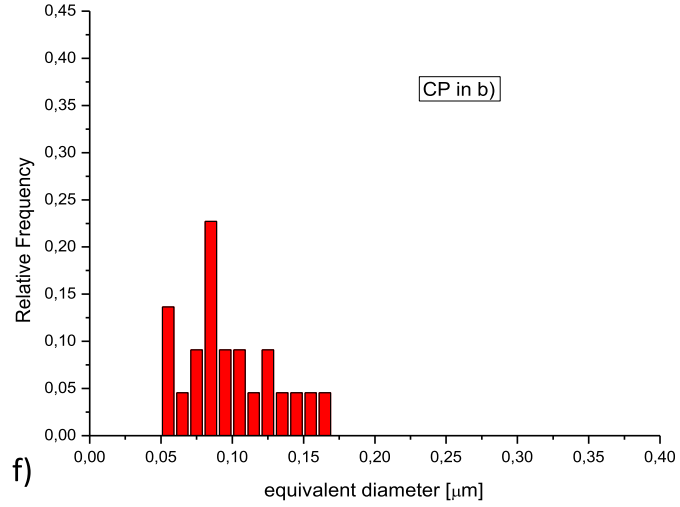

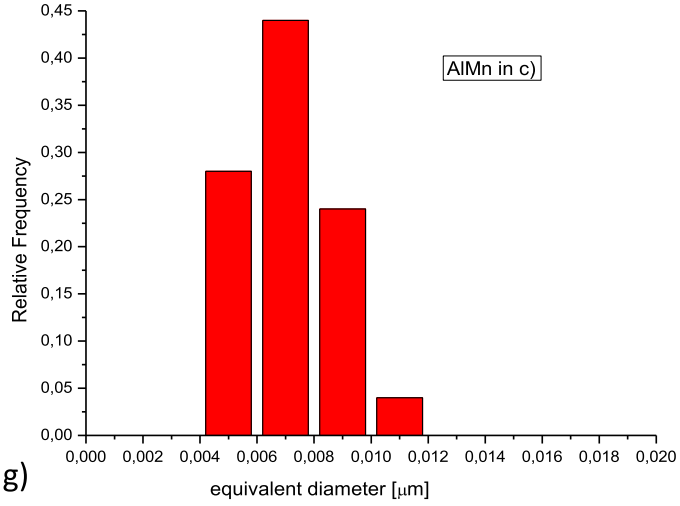

Fig. 14. (*continued*)

considered only the CP particle strengthening. This is obvious by considering that one sample has been deformed at high temperature and recovery mechanisms have occurred, leading to a stronger decrease in strength compared to 2500-30 deformed at room temperature. For Vickers hardness the situation is reversed, as shown in Fig. 8. Hardness data, collected at room temperature, illustrate a strengthening in the middle of the nugget. The increment in HV of the sample deformed at 350 °C is 13%–15% compared to the 2500-30 (as FSPed). Since the strengthening contribution coming from particles is not so

Please cite this article in press as: E. Cerri, D. Knez, T. Rimoldi, M.T. Di Giovanni, Microstructure evolution and mechanical properties of hot deformed Mg9Al1Zn samples containing a friction stir processed zone, Journal of Magnesium and Alloys (2017), doi: 10.1016/j.jma.2017.11.003

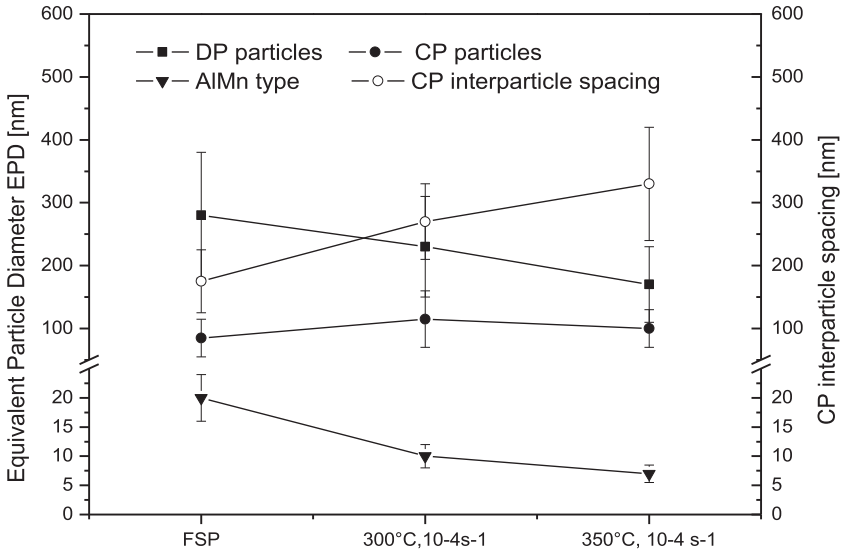

Fig. 15. Equivalent particle diameter (EPD) evolution and inter-particle spacing of continuous precipitated (CP) particles during tensile test at high temperature.

effective according to previous calculations, the important rise in HV (Fig. 8) has to be related to solid solution strengthening and strain hardening mechanisms.

4. Conclusions

The effects of hot deformation on HPDC AZ91 subjected to friction stir processing were analysed. Several process conditions were experimented but just one was chosen (2500 rpm and 30 mm/min) for performing mechanical tests at high temperature. In order to characterise the microstructure after tensile tests at 300 °C and 350 °C, a deep study was first performed on the as friction stir processed samples. The main findings are summarised in the followings.

- The hot deformation at 350 °C induces a ductility that is doubled compared to samples deformed at 300 °C and strengthens the nugget region, as measured by microhardness profiles, compared to as FSP sample. Hardness and average grain size were correlated by a Hall–Petch type equation by considering local values.
- TEM observations have allowed particle investigations; DP and CP are still present after FSP and after tensile tests. Statistical evaluation of equivalent particle diameter in DP and CP lead to definition of particle evolution as function of temperature. EDS and EELS identified the particle type as MgAlZn and AlMn type particles. Exposure to high temperature (350 °C) of AlMn leads to a decrease of their size to 7 nm.
- The strengthening in HV measured in the nugget after hot deformation has been ascribed mainly to solid solution strengthening and strain hardening.

Acknowledgements

Financial support from ESTEEM2 project at FELMI-Graz is gratefully acknowledged. Special thanks to Mr. D. Ciccarelli for technical assistance.

References

[1] Z.Y. Ma, A.L. Pilchak, M.C. Juhas, J.C. Williams, Scripta Mater. 58 (2008) 361–366.
[2] U.F.H.R. Suhuddin, S. Mironov, Y.S. Sato, H. Kokawa, C.W. Lee, Acta Mater. 57 (2009) 5406–5418.
[3] V. Jain, J.Q. Su, R.S. Mishra, R. Verma, A. Javaid, M. Aljarrah, E. Essadiqui, in: W.H. Sillekens, et al. (Eds.), Magnesium Technology, TMS, Warrendale, PA, 2011, pp. 205–209.
[4] C.I. Chang, X.H. Du, J.C. Huang, Scripta Mater. 57 (2007) 209–212.
[5] S.H.C. Park, Y.S. Sato, H. Kokawa, Metall. Mater. Trans. A 34 (2003) 987–994.
[6] W. Yuan, R.S. Mishra, Mater. Sci. Eng. A 558 (2012) 716–724.
[7] Z. Yu, H. Choo, Z. Feng, S.C. Vogel, Scr. Mater. 63 (2010) 1112–1115.
[8] C.I. Chang, C.J. Lee, J.C. Huang, Scripta Mater. 51 (2004) 509–514.
[9] H. Watanabe, T. Mukai, K. Ishikawa, M. Mabuchi, K. Higashi, Mater. Sci. Eng. A 307 (2001) 119–128.
[10] A. Mohan, W. Yuan, R.S. Mishra, Mat. Sci. Eng. A 562 (2013) 69–76.
[11] V. Jain, R.S. Mishra, J. Mat. Sci. 48 (2013) 2635–2646.
[12] F. Chai, D. Zhang, Y. Li, W. Zhang, Mat. Sci. Eng. A 568 (2013) 40–48.
[13] J.A. del Valle, P. Rey, D. Gesto, D. Verdera, J.A. Jiménez, O.A. Ruano, Mat. Sci. Eng. A 628 (2015) 198–206.
[14] A.H. Feng, Z.Y. Ma, Scripta Mater. 56 (2007) 397–400.
[15] P. Cavaliere, P.P. De Marco, J. Mater. Proc. Technol. 184 (2007) 77–83.
[16] E. Cerri, M. Cabibbo, P. Leo, La Metallurgia Italiana vol5 (2014) 3–10.
[17] E. Cerri, P. Leo, Mat. Sci. Forum 783–786 (2014) 1735–1740.
[18] E. Cerri, G. Renna, M. Cabibbo, M. Simoncini, A. Forcellese, Mat. Sci. Forum 879 (2017) 295–300.
[19] E. Cerri, M.T. Di Giovanni, T. Rimoldi, L. Cristofolini, Mat. Sci. Forum 879 (2017) 301–305.
[20] R.S. Mishra, Z.Y. Ma, Mater. Sci. Eng. R. 50 (2005) 1–78.
[21] B.D. Cullity, S.R. Stock, Elements of X-Ray Diffraction, third ed., Pearson Education Ltd, 2014.
[22] http://etheses.bham.ac.uk/4695/9/Zeng13PhD.pdf.
[23] R. Zeng, Precipitation hardening inAZ91 magnesium alloy, (Ph.D. candidate thesys), University of Birmingham; 2013.
[24] S. Celotto, T.J. Bastow, Acta Mater. 49 (2001) 41–51.
[25] R. Zeng, Y. Chiu, I.P. Jones, J. All. Comp. 579 (2013) 34–38.
[26] C.R. Hutchinson, J.F. Nie, S. Gorsse, Metall. Mater. Trans. A 36 (2005) 2093–2105.
[27] W. Yuan, S.K. Panigrahi, R.S. Mishra, Metall. Mater. Trans. A 44 (2013) 3675–3684.
[28] L.M. Brown, R.K. Ham, in: A. Kelly, R.B. Nicholson (Eds.), Elsevier London, 1971, p. 12.

Please cite this article in press as: E. Cerri, D. Knez, T. Rimoldi, M.T. Di Giovanni, Microstructure evolution and mechanical properties of hot deformed Mg9Al1Zn samples containing a friction stir processed zone, Journal of Magnesium and Alloys (2017), doi: 10.1016/j.jma.2017.11.003